Electron-electron and electron-phonon correlation effects on the finite temperature electronic and optical properties of zb-GaN

Hiroki Kawai, Koichi Yamashita, Elena Cannuccia, Andrea Marini

Electron–electron and electron–phonon correlation effects on the finite temperature electronic and optical properties of *zb*–GaN

Hiroki Kawai,[1] Koichi Yamashita,[1] Elena Cannuccia,[2] and Andrea Marini[3,4]

[1] *Department of Chemical System Engineering, School of Engineering, The University of Tokyo, Tokyo 113-8656, Japan*
[2] *Institut Laue Langevin BP 156 38042 Grenoble France*
[3] *Istituto di Struttura della Materia of the National Research Council, Via Salaria Km 29.3, I-00016 Monterotondo Stazione, Italy*
[4] *European Theoretical Spectroscopy Facilities (ETSF)*

(ΩDated: August 11, 2018)

We combine the effect of the electron–electron and electron–phonon interactions to study the electronic and optical properties of *zb*–GaN. We show that only by treating the two effects at the same time it is possible to obtain an unprecedented agreement of the zero and finite–temperature electronic gaps and absorption spectra with the experimental results. Compared to the state–of–the–art results our calculations predict a large effect on the main absorption peak position and width as well as on the overall absorption lineshape. These important modifications are traced back to the combined electron–phonon damping mechanism and non uniform *GW* level corrections. Our results demonstrate the importance of treating on equal footing the electron and phonon mediated correlation effects to obtain an accurate description of the III–nitrides group physical properties.

PACS numbers: 71.38.-k, 78.20.-e, 63.20.dk, 65.40.-b

I. INTRODUCTION

The group III–nitride semiconductors, i.e., GaN, AlN, InN and their alloys are materials with many applications in the field of optoelectronics. These include, among others, light emitting diodes (LEDs), laser diodes (LDs), heterojuction field–effect transistors (HFETs)[1–5]. This class of compounds is widely used being characterized by the most stable wurtzite structure. They have built–in electric fields arising from the spontaneous and piezoelectric polarization along the *c* axis. These fields are, however, undesirable in the applications of the heterostructures as quantum wells (QWs) or superlattices since they complicate the design and worsen the sample malleability. One of the approaches to eliminate these internal fields is the utilization of metastable non polar zinc–blende (*zb*) structures. It has also been reported that *zb* group III–nitrides have a quantum confined Stark effect in low–dimensional heterostructures[6], high *p*–type conductivity in (Ga,Mn)N thin films[7] and negative differential resistance (NDR) at the resonant tunneling diode of the cubic Al(Ga)N/GaN[8,9]. Consequently a lot of interest is constantly attracted by this family of materials.

In last few years *zb*–GaN with high phase–purity and crystalline quality has been fabricated as a nearly strain–free epitaxial layer on 3C-SiC(001)/Si pseudo substrates by plasma–assisted molecular beam epitaxy[6,9–11]. This experimental achievement boosted the interest on fundamental optical properties as photoluminescence, photoreflectance and ellipsometry with particular attention on their temperature dependence.

In contrast to such abundance of experimental results the agreement with the state–of–the–art calculations of the optical properties of *zb*–GaN is still not satisfactory. In these approaches the absorption spectrum is calculated[12] by including electron–hole interaction by solving the Bethe–Salpeter equation (BSE) derived within the Many–Body Perturbation Theory (MBPT)[13]. Nevertheless the main peak position is strongly underestimated when compared to the experimental result. And also the complex temperature dependence observed experimentally is not captured at all. Similarly, the band structure of *zb*–GaN has been deeply investigated by using the most up–to–date theoretical approaches. In this case electron–electron correlation only has been included, by means of the well known *GW* approximation[14]. The corresponding quasi–particle (QP) gap, calculated by using the one–shot *GW* approximation on top of Kohn–Shame (KS) HSE hybrid orbital (HSE+G_0W_0)[6,15], is 3.427 eV, which overestimates the experimental value of 3.295 eV[6].

The common denominator to these calculations of the electronic and optical properties is that electron–phonon (EP) interaction is not considered. As a natural consequence no temperature dependence is captured. And, more importantly, also the well–known zero–point motion effect is neglected. This assumption is, on the basis of very recent results[16–20], not well–motivated. Indeed the majority of the *ab-initio* simulations of the electronic and optical properties of a wide class of materials are generally performed by keeping the atoms frozen in their crystallographic positions. Nevertheless, many years ago, Heine, Allen, and Cardona (HAC)[21,22] pointed out the fact that the electronic states can be strongly affected by the lattice vibrations even when $T \to 0\,\mathrm{K}$ through the quantum zero–point motion effect. In the HAC approach the EP interaction is treated in a static manner and the atomic displacements are considered as static perturbations. The HAC approach successfully explained the temperature dependence of the gap shift and peak broadening in semiconductors like Si or Ge[23] . BSE calculations on top of QP states including EP correc-

tion have also been performed, showing remarkable EP effect on the excitonic states and explaining the finite temperature evolution of the optical absorption measured experimentally[24].

Despite of these successful results based on the HAC approach it has been recently discovered the key importance of considering dynamical corrections to the static HAC picture. For instance, diamond has been shown to have large dynamical EP effects, which explain the subgap states observed experimentally in the absorption spectrum[17]. Similarly, carbon polymer systems like *trans*–polyacetylene and polyethylene, show a severe breakdown of the QP picture induced by the EP interaction[17,18].

In this work we calculate the electronic and optical properties of *zb*–GaN by including electron–phonon and electron–electron interaction. Our results show a remarkable impact of electron–phonon interaction even at zero–temperature which corrects the overestimation of the QP gap obtained within the HSE+G_0W_0 method. At the same time we prove that only by treating on the same level electron–electron and electron–phonon interactions it is possible to obtain and unprecedented agreement with experiment result, both at zero and finite temperature.

The paper is organized as following. In Sec.II the EP interaction is briefly discussed in a MBPT framework. In Sec.III the electronic gap and transition energies at high–symmetry points of the Brilloun zone of *zb*–GaN are studied. In Sec.IV we analyze the zero and finite temperaturs optical absorption by including both electron–hole attraction and electron–phonon effects by using the BSE.

II. A MANY–BODY PERTURBATION THEORY APPROACH TO THE ELECTRON–PHONON PROBLEM

The total Hamiltonian of the coupled electron–nuclei system $\hat{H}$ can be divided into three parts

$$\widehat{H} = \widehat{H}_0 + \widehat{H}_1 + \widehat{H}_2, \tag{1}$$

where $\hat{H}_0$ is the electronic Hamiltonian corresponding to the case where the atoms are frozen at their equilibrium positions $\mathbf{R}_0$,

$$\widehat{H}_0 = \sum_i \left[-\frac{1}{2}\frac{\partial^2}{\partial \hat{\mathbf{r}}_i{}^2} + \hat{V}_{ion}\left[\{\mathbf{R}\}\right]\Big|_{\mathbf{R}=\mathbf{R}_0}(\mathbf{r}_i) \right] + \hat{W}_{e-e}. \tag{2}$$

$\widehat{H}_1$ and $\widehat{H}_2$ represent, respectively, the first and second term in the Taylor expansion of $\widehat{H}_0$ when the atomic positions $\{\mathbf{R}\}$ are expanded around the equilibrium positions $\{\mathbf{R}_0\}$. At this stage electron–electron correlations (described by $\hat{W}_{e-e}$) are treated at a mean–field level by using the standard Density–Functional Theory (DFT). In DFT $\widehat{H}_0 \approx \sum_i \left[\hat{h}(\mathbf{r}_i)\right]$ with

$$\hat{h}(\mathbf{r}) = -\frac{1}{2}\frac{\partial^2}{\partial \hat{\mathbf{r}}^2} + \hat{V}_{scf}\left[\{\mathbf{R}\}\right]\Big|_{\mathbf{R}=\mathbf{R}_0}(\mathbf{r}), \tag{3}$$

and the derivatives of the electronic effective potential $\widehat{V}_{scf} = \widehat{V}_{ion} + \widehat{V}_H + \widehat{V}_{xc}$ with respect to the atomic coordinates $\mathbf{R}$ can be calculated, self–consistently, by using Density–Functional Perturbation Theory (DFPT).

Within MBPT[17,18] the exact single particle excitation energies of the total Hamiltonian $\widehat{H}$ are obtained as poles of the Green's Function[25] $G_{n\mathbf{k}}(\omega)$ that is solution of the Dyson Equation:

$$G_{n\mathbf{k}}(\omega) = G^{(0)}_{n\mathbf{k}}(\omega)\left[1 + \Sigma_{n\mathbf{k}}(\omega) G_{n\mathbf{k}}(\omega)\right]. \tag{4}$$

MBPT allows to calculate Σ in terms of $\widehat{H}_1$ and $\widehat{H}_2$. We consider now the two lowest–order non–vanishing contributions to Σ written as functionals of the non–interacting Green's function $G^0_{n\mathbf{k}}(\omega)$. The second–order term in the perturbative expansion in powers of $\widehat{H}_1$ gives the Fan contribution[26] to the self–energy

$$\Sigma^{Fan}_{n\mathbf{k}}(\omega, T) = \sum_{n'\mathbf{q}\lambda} \frac{\mid g^{\mathbf{q}\lambda}_{nn'\mathbf{k}} \mid^2}{N_q} \times \\ \times \left[\frac{N_{\mathbf{q}\lambda}(T) + 1 - f_{n'\mathbf{k}-\mathbf{q}}}{\omega - \varepsilon_{n'\mathbf{k}-\mathbf{q}} - \omega_{\mathbf{q}\lambda} - i0^+} + \right. \\ \left. + \frac{N_{\mathbf{q}\lambda}(T) + f_{n'\mathbf{k}-\mathbf{q}}}{\omega - \varepsilon_{n'\mathbf{k}-\mathbf{q}} + \omega_{\mathbf{q}\lambda} - i0^+} \right], \tag{5}$$

where $\varepsilon_{n'\mathbf{k}-\mathbf{q}}$ is Kohn–Sham energy of the n'th band at the point $\mathbf{k}-\mathbf{q}$ in the Brillouin zone. $\omega_{\mathbf{q}\lambda}$ is phonon energy relative to the mode λ and transferred momentum $\mathbf{q}$. $N_{\mathbf{q}\lambda}(T)$ is the Bose–Einstein distribution function of the phonon mode $(\mathbf{q},\lambda)$ at temperature T and $f_{n'\mathbf{k}-\mathbf{q}}$ is the occupation number of the bare electronic state at $(n', \mathbf{k}-\mathbf{q})$. $g^{\mathbf{q}\lambda}_{n'n\mathbf{k}}$ are the electron–phonon matrix element[18] defined as:

$$g^{\mathbf{q}\lambda}_{nn'\mathbf{k}} = \sum_{s\alpha} (2M_s\omega_{\mathbf{q}\lambda})^{-1/2} e^{i\mathbf{q}\cdot\tau_s} \times \\ \times \langle n\mathbf{k}|\frac{\partial \widehat{V}_{scf}(\mathbf{r})}{\partial R_{s\alpha}}|n'\mathbf{k}-\mathbf{q}\rangle \xi_\alpha(\mathbf{q}\lambda|s), \tag{6}$$

with M_s the mass of the atom whose position in the unit cell is τ_s. $\xi_\alpha(\mathbf{q}\lambda|s)$ are the phonon polarization vectors. As already pointed out all ingredients of Eq.(6) are calculated by using DFPT.

Similarly to the Fan term, the Debye–Waller (DW) self–energy arises from the first–order term in the perturbative expansion in powers of $\widehat{H}_2$,

$$\Sigma^{DW}_{n\mathbf{k}}(T) = \frac{1}{N_q}\sum_{\mathbf{q}\lambda} \Lambda^{\mathbf{q}\lambda,-\mathbf{q}\lambda}_{nn\mathbf{k}}(2N_{\mathbf{q}\lambda}(T) + 1), \tag{7}$$

where $\Lambda^{\mathbf{q}\lambda,-\mathbf{q}\lambda}_{nn\mathbf{k}}$ is a second–order electron–phonon matrix element[18]:

$$\Lambda^{\mathbf{q}\lambda,\mathbf{q}'\lambda'}_{nn'\mathbf{k}} = \frac{1}{2}\sum_{s}\sum_{\alpha,\beta}\frac{\xi^{*}_{\alpha}(\mathbf{q}\lambda|s)\,\xi_{\beta}(\mathbf{q}'\lambda'|s)}{2M_{s}\left(\omega_{\mathbf{q}\lambda}\omega_{\mathbf{q}'\lambda'}\right)^{1/2}}\times \\ \times\langle n\mathbf{k}|\frac{\partial^{2}\widehat{V}_{scf}(\mathbf{r})}{\partial R_{s\alpha}\partial R_{s\beta}}|n'\mathbf{k}-\mathbf{q}-\mathbf{q}'\rangle. \quad (8)$$

By solving explicitly Eq.(4) the fully interacting Green's function $G_{nk}(\omega,T)$ can be written as

$$G_{n\mathbf{k}}(\omega,T) = \frac{1}{\omega-\varepsilon_{n\mathbf{k}}-\Sigma^{Fan}_{n\mathbf{k}}(\omega,T)-\Sigma^{DW}_{n\mathbf{k}}(T)}. \quad (9)$$

The imaginary part of the Green's function $A_{n\mathbf{k}}(\omega,T)\equiv\pi^{-1}\mid\Im\left[G_{n\mathbf{k}}(\omega,T)\right]\mid$ gives the electronic spectral function (SF). In the quasi–particle approximation (QPA) the SF is assumed to be well described by a lorentzian function. Mathematically this means that the self–energy frequency dependence can be expanded linearly around the bare electronic energy. In this case, the pole of $G_{nk}(\omega,T)$, $E_{n\mathbf{k}}(T)$ is given by

$$E_{n\mathbf{k}}(T) = \varepsilon_{n\mathbf{k}}+ \\ + Z_{n\mathbf{k}}(T)\left[\Sigma^{Fan}_{n\mathbf{k}}(\varepsilon_{n\mathbf{k}},T)+\Sigma^{DW}_{n\mathbf{k}}(T)\right], \quad (10)$$

with $Z_{n\mathbf{k}}(T) = \left(1-\frac{\partial\Sigma^{Fan}_{n\mathbf{k}}(\omega,T)}{\partial\omega}\Big|_{\omega=\varepsilon_{n\mathbf{k}}}\right)^{-1}$ representing the renormalization factor. The on–the–mass–shell (OMS) approximation represents the static limit of the QPA, obtained by assuming $\Sigma^{Fan}_{n\mathbf{k}}(\omega,T)\approx\Sigma^{Fan}_{n\mathbf{k}}(\omega,T)\big|_{\omega=\varepsilon_{n\mathbf{k}}}$, which is equivalent to assume $Z_{n\mathbf{k}}(T)=1$ in the QPA. The Fan and DW self–energies are complex and real functions, respectively, thus the former gives both an EP induced energy shift and broadening while the latter contributes only with a constant energy shift. Both self–energies depend explicitly on the temperature T via the $N_{\mathbf{q}\lambda}(T)$ factor.

III. RENORMALIZATION OF THE SINGLE PARTICLE ENERGY LEVELS. THE COMBINED EFFECT OF THE ELECTRON–ELECTRON AND ELECTRON–PHONON INTERACTIONS

zb–GaN is a polar material and, as a consequence, large static EP effects are expected[27]. As mentioned above a strong EP coupling can eventually induce the breakdown of the QPA. A clear and simple way to test the QPA validity is to calculate the renormalization factors $Z_{n\mathbf{k}}(T)$. Indeed, by using Eq.(9) and Eq.(10) it turns out that, within the QPA, the Green's function $G^{QP}_{n\mathbf{k}}(\omega,T)$ can be written as

$$G^{QP}_{n\mathbf{k}}(\omega,T) = \frac{Z_{n\mathbf{k}}(T)}{\omega-E_{n\mathbf{k}}(T)}, \quad (11)$$

with $E_{n\mathbf{k}}(T)$ evaluated by means of Eq.(10). When $Z_{n\mathbf{k}}=1$ the SF, $\Im|G^{QP}_{n\mathbf{k}}(\omega,T)|$, reduces to a lorentzian function with a pole at $\omega=\Re\left[E_{n\mathbf{k}}(T)\right]$ and width $\Gamma_{n\mathbf{k}}(T)=\Im\left[E_{n\mathbf{k}}(T)\right]$. Thus, the $Z_{n\mathbf{k}}$ values measure the strength of the quasi–particle pole, i.e., the QP picture is well motivated when the SF can be well approximated with a single Lorentzian–like function.

In our EP calculations the optimized geometry and the electronic state are obtained by using the PWSCF code[28]. Electron–phonon calculations are performed with the Yambo code[29] by using the phonons frequencies and $g^{\mathbf{q}\lambda}_{nn'\mathbf{k}}$ matrix elements calculated with PWSCF within DFPT. As a results of our simulations the majority of the states that contribute to the optical absorption are well described by Lorentzian–like SF, as shown in Fig.1. In addition most of the states show values of $Z_{n\mathbf{k}}$ very close to 1. For example, the states corresponding to the valence band maximum (VBM) and the conduction band minimum (CBM) at the Γ point, have $Z_{n\mathbf{k}}=0.91$ and $Z_{n\mathbf{k}}=0.98$, respectively.

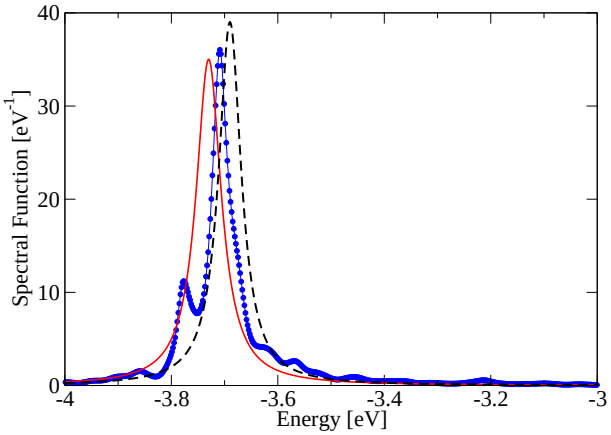

FIG. 1. Spectral function of a valence band state. This well represents the general trend of the majority of spectral functions covering the energy range involved in the absorption process, as discussed in the text. Blue line with dots is the calculated SF. This is compared with two Lorentzian functions corresponding to the OMS (red solid line) and to the QPA (black dash line). Both approximation reproduce the calculated SF quite well and the use of the OMS is, therefore, well motivated.

This indicates that, in *zb*–GaN, the OMS approximation is well motivated and most of the weight can be safely assumed to be in one single peak. There is, however, another and more stringent motivation in favor of OMS as far as the calculation of the optical properties is concerned. A $Z_{n\mathbf{k}}$ factor smaller than 1 is known to reduce the intensity of the absorption spectrum. At the same time, however, it is well known that such reduction is compensated by the dynamical electron–hole interactions[30,31]. As far as these dynamical effects are neglected (as commonly done in the state–of–the–art implementation of the BSE used in this work) the OMS assumption of $Z_{n\mathbf{k}}=1$ is well motivated also from a purely theoretical point of view.

In order to describe the impact of EP on the electronic states we consider the energies corresponding to the lowest transition energies at several high–symmetry points. These energies are compared with the experimental results in Tab. I. DFT is well known to underestimate the band gaps of about $\simeq 40\%$. In fact, our DFT calculation (performed with the LDA) yields 2.231 eV as the band gap of *zb*–GaN. This is clearly less than the experimental value, that is 3.295 eV at 10 K[6]. Our LDA+G_0W_0 calculations within the plasmon–pole approximation[14] opens the gap to 3.239 eV, which well agrees with the experiment. Still, the combination LDA+G_0W_0 largely underestimates the transition energies at L and X.

This underestimation can be traced back to the local treatment of electron–electron correlation effects in the self–consistent DFT–LDA calculation. This limitation can be overcome by using the AM05[32] approximation for the exchange–correlation energy functional to calculate the optimized geometry and the HSE[33] functional for the start point of G_0W_0 calculation.

From Tab. I it is evident that HSE+G_0W_0 overestimates the transition energies at all three high symmetry points[15]. At the same time, however, the EP interaction greatly reduces this overestimation leading to an excellent agreement with the experimental results. Our calculation at OMS level gives a gap correction of -0.127 eV at Γ, which reduces the HSE+G_0W_0 gap to 3.300 eV, in agreement with the experiment. Similarly, at the L and X points, the EP induced correction is -0.190 eV and -0.132 eV resulting in transition energies of 7.517 eV and 7.624 eV, again in very good agreement with the experiment. This result indicates the importance of the EP correction in *zb*–GaN, pointing to similar and potentially important corrections in the whole III–nitrides group of materials.

TABLE I. Lowest transition energies at high–symmetry points in the Brillouin zone of *zb*–GaN. The values obtained from LDA, LDA+G_0W_0, HSE+G_0W_0[15] and HSE+G_0W_0+OMS calculations are compared with the experimental values[6]. All values are in eV.

	Γ	L	X
LDA	2.231	5.952	6.034
LDA+G_0W_0	3.239	7.117	7.105
HSE+G_0W_0	3.427	7.707	7.755
HSE+G_0W_0+OMS	3.300	7.517	7.624
Exp ($T = 10$ K)	3.295	7.33[a]	7.62[a]

[a] Excitation peak energies.

IV. FINITE TEMPERATURE OPTICAL ABSORPTION SPECTRA INCLUDING ELECTRON–HOLE EFFECTS

The optical absorption spectrum is defined as the imaginary part of the macroscopic dielectric function $\Im\left[\epsilon_M\left(\omega\right)\right]$. This can be easily expressed, in the long wave length limit, as

$$\epsilon_M\left(\omega\right) = 1 - \lim_{\mathbf{q}\to 0} v_0\left(\mathbf{q}\right) \int d\mathbf{r} d\mathbf{r}' e^{-i\mathbf{q}\left(\mathbf{r}-\mathbf{r}'\right)} \overline{\chi}\left(\mathbf{r},\mathbf{r}';\omega\right), \quad (12)$$

with $v_{\mathbf{G}}\left(\mathbf{q}\right) = 4\pi/|\mathbf{G}+\mathbf{q}|^2$ the Coulomb potential and $\overline{\chi}\left(\mathbf{r};\mathbf{r}';\omega\right)$ the two–point polarizability. The equation of motion for the polarizability[13] can be rewritten by introducing a single–particle basis set ($\{\phi_{n,\mathbf{k}}\}$) to expand the density operator. This is equivalent to define the electron–hole probability functions $\Phi_{\mathbf{K}}\left(\mathbf{r}\right) = \phi_{c\mathbf{k}}\left(\mathbf{r}\right)\phi^*_{v\mathbf{k}}\left(\mathbf{r}\right)$. Here $\mathbf{K}$ represents the general conduction–valence pairs, $\mathbf{K} = (c, v, \mathbf{k})$. In this basis $\overline{\chi}$ is

$$\overline{\chi}\left(\mathbf{r};\mathbf{r}';\omega\right) = -\left(\frac{i}{\Omega N}\right) \sum_{\mathbf{K}_1,\mathbf{K}_2} \Phi^*_{\mathbf{K}_1}\left(\mathbf{r}\right) L_{\mathbf{K}_1\mathbf{K}_2}\left(\omega\right) \Phi_{\mathbf{K}_2}\left(\mathbf{r}'\right). \quad (13)$$

Eq.(13) introduces the electron–hole Green's function $L_{\mathbf{K}_1\mathbf{K}_2}\left(\omega\right)$ that satisfies the BSE equation[13]

$$L_{\mathbf{K}_1\mathbf{K}_2}\left(\omega\right) = L^0_{\mathbf{K}_1\mathbf{K}_2}\left(\omega\right) + L^0_{\mathbf{K}_1\mathbf{K}_3}\left(\omega\right) \Xi_{\mathbf{K}_3\mathbf{K}_4}\left(\omega\right) L_{\mathbf{K}_4\mathbf{K}_2}\left(\omega\right). \quad (14)$$

The Bethe–Salpeter kernel Ξ is defined as $\Xi = -iV + iW$ with V and W the exchange and screened Coulomb interactions, respectively. $L^0_{\mathbf{K}_1\mathbf{K}_2}\left(\omega\right)$, in Eq.(14), is the free electron–hole Green's function, defined in Eq.(15).

As previously described by Marini[24] it is possible to include finite–temperature effect in the BSE by using, as reference single–particle energies, the temperature–dependent and complex QP energies $E_{n\mathbf{k}}\left(T\right)$. In this way the free electron–hole Green's function $L^0_{\mathbf{K}_1\mathbf{K}_2}\left(\omega, T\right)$ depends explicitly on the temperature

$$L^0_{\mathbf{K}_1\mathbf{K}_2}\left(\omega, T\right) = i\left[\frac{f_{c_1\mathbf{k}_1} - f_{v_1\mathbf{k}_1}}{\omega - E_{c_1\mathbf{k}_1}\left(T\right) + E_{v_1\mathbf{k}_1}\left(T\right) + i0^+}\right] \delta_{\mathbf{K}_1\mathbf{K}_2}. \quad (15)$$

Eq.(15) ensures that also the fully interacting electron–hole Green's function and the absorption spectra depend explicitly on the temperature, thanks to Eq.(12) and Eq.(13).

In order to solve the BSE we adopt two standard approximations. The first is the Tamm–Dancoff approximation which corresponds to neglect the coupling between the resonant and the anti–resonant part of the BSE kernel. The second is the use of a statically screened electron–hole potential W.

In Fig.2 we show the calculated absorption spectrum. In addition to the G_0W_0 corrections calculated as described in Sec.III we include EP effects. To obtain a converged absorption spectra we employed the random–integration method (RIM)[29] by selecting around 30000

random **k**-points in the whole Brillouin Zone. The resulting spectrum (thick black line) is compared to the previous calculation of Benedict *et al.*[12] (dashed red line) which is performed in a LDA basis without including the EP interaction. The present calculation, instead, is in excellent agreement with the $T = 10K$ experimental spectrum[6] (green bold line) and largely improves the Benedict result. We notice, indeed, that, compared to the Benedict calculation, the position and width of the main peak is in very good agreement with the experiment. This pronounced peak located at around 7.62 eV is due to interband transitions in a region of the Brillouin Zone near the X point. These transitions extend to regions where the valence and conduction bands are parallel with a similar energy distance.

It is crucial to underline that, in the present work, the absorption spectrum width is dictated by the EP interaction and it is temperature–dependent. Indeed we only use a very small artificial damping (10 meV) in Eq.(15) to avoid numerical instabilities. Compared to the case of Benedict, where this broadening is arbitrarily chosen to be 200 meV, the EP interaction correctly describes both the main peak and the steep absorption edge.

Finally we investigate how the optical spectrum evolves as the temperature is increased. In Fig. 3 we show the calculated absorption spectra at $T = 0$ K, 300 K and 600 K. In the first two cases the numerical simulation is compared with the available experimental results[6]. The agreement is fairly good and confirms that the present approach is able to correctly capture the finite temperature effects. The energy shifts of the first excitation peaks due to electron–hole transitions occurring at Γ, L and X is experimentally -63 meV, -100 meV and -110 meV when the temperature is increased from 10 K to 295 K[6]. Our calculations give -83 meV, -144 meV, and -106 meV, respectively, which show a quntitative agreement with experiment. Also the general trend observed experimentally that the peak shift is larger at critical points with higher transition energy is reproduced.

On the other hand, from Fig.3 we deduce that the broadening of the main peak at the X point is slightly overestimated at $T = 300$ K compared to the experiment. In order to understand the source of this overestimation we notice that, in the QP picture, the EP induced broadening of the valence band top and conduction band bottom at the X point are 121.8 meV and 12.1 meV at $T = 300$ K. In the independent particle approximation (where $L_{\mathbf{K}_1\mathbf{K}_2} \approx L^0_{\mathbf{K}_1\mathbf{K}_2}\delta_{\mathbf{K}_1\mathbf{K}_2}$) the electron–hole broadening is simply the sum of the two. Now, as also in the case where electron–hole attraction is included, the main absorption peak originates from transitions concentrated around the VBM and CBM we deduce that the overestimation is due to a too large broadening of the underlying QP states.

In the experimental work by Logothetidis *et al.*[34] the broadening at the main absorption peak is described by

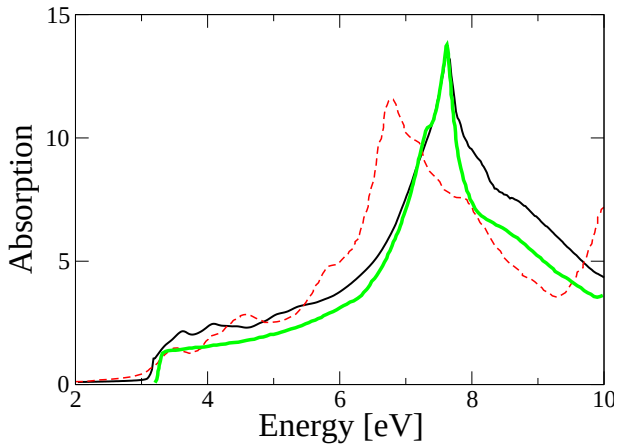

FIG. 2. Theoretical and experimental absorption spectra of *zb*–GaN at $T = 10\,K$. The spectrum obtained by solving the BSE including the EP correction (black thin line) is in excellent agreement with the experimental result[6] (green bold line). Compared to the state–of–the–art calculation of Benedict *et al.*,[12] (dashed red line) the agreement is largely improved.

a phenomenological model

$$\Gamma(T) = \Gamma_1 + \Gamma_0 \left[1 + \frac{2}{\exp(\Theta/T) - 1}\right], \qquad (16)$$

with $\Gamma_1 = 27$ meV, $\Gamma_0 = 44$ meV, and $\Theta = 522$ K. The first term in Γ_1 is to describe temperature–independent mechanism, as surface scattering, thus we set it to 0 to compare Eq.(16) with our theoretical results. Eq.(16), indeed, predicts $\Gamma(T = 300) \sim 62.7$ meV that is half of the value that results from the solution of the BSE.

A reasonable explanation of this deviation is in the underlying unperturbed band structure. The band curvature has a large impact on the EP induced broadening through the denominator of Eq.(5), especially by the dominant intraband–scattering terms with $\omega = \varepsilon_{n\mathbf{k}}$, $n' = n$, and small $\mathbf{q}$. Since our EP self–energies are calculated on top of Kohn–Sham states from LDA, the resulted band widths are too small. As shown in previous calculations[15] the valence band at the X point is characterized by a large curvature that is underestimated by the LDA calculations. We expect that the broadening would be improved by an EP calculations performed on top of HSE+G_0W_0 band structure, but it is prohibitively expensive from the computational point of view. Nevertheless our approach, based on LDA, gives excellent results especially at the low temperature.

V. CONCLUSION

In this work we study the zero and finite temperature electronic and optical properties of *zb*–GaN. The effect of electron–phonon interaction,treated in a fully dynamical approach based on the Many–Body Perturbation Theory, shows that the simple on–the–mass–shell approximation

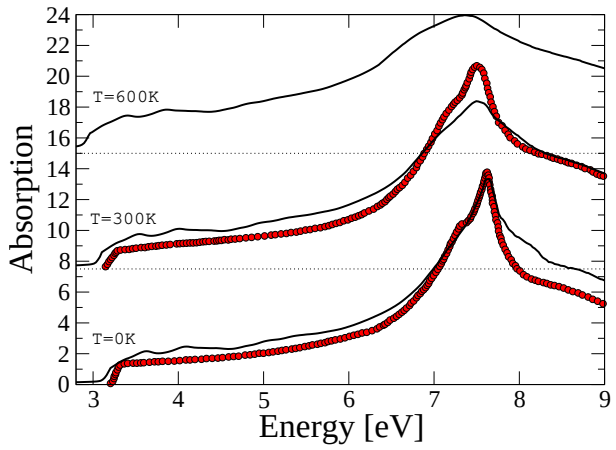

FIG. 3. Absorption spectra of *zb*–GaN at $T = 0$, 300, and 600 K. Red circles are experimental results at 10 K and 295 K.[6]

to the quasi–particle energies and widths is well motivated for the low energy states involved in the absorption spectrum.

By including, in an *ab-initio* manner, the combined effect of the electron–electron and the EP interaction we obtain an excellent agreement with the experimental foundamental band gaps.

The solution of the BSE calculated on top of the HSE+G_0W_0 band structure including EP effects leads to an excellent agreement also for the optical absorption spectrum measured on high phase–purity samples. Both the position and the broadening of the most intense absorption peak are correctly reproduced in the low–temperature regime. In the room–temperature case, instead, the red–shift of the main peak position is well described while the broadening is sliglhtly overestimated. Despite this overestimation the present results still represent a major improvement with respect to the state–of–the–art simulations.

Our results clearly point to the crucial important of including at the same time electron–electron and electron–phonon correlation effects for a comprehensive and quantitative understanding of the electronic and optical properties of group III–nitrides.

ACKNOWLEDGMENTS

H. K is supported by JSPS Research Fellowships for Young Scientists and JSPS KAKENHI (24-7666). A. M. acknowledges funding by MIUR FIRB Grant No. RBFR12SW0J.

[1] D. J. As, Microelectron J. **40**, 204 (2009).
[2] S. V. Novikov *et al.*, Semicond. Sci. Technol. **23**, 015018 (2008).
[3] O. Ambacher *et al.*, J. Phys.: Condens. Matter. **14**, 3399 (2002).
[4] E. Tschumak *et al.*, Appl. Phys. Lett. **96**, 253501 (2010).
[5] C. Mietze *et al.*, Phys. Rev. B **83**, 195301 (2011).
[6] M. Feneberg *et al.*, Phys. Rev. B **85**, 155207 (2012).
[7] K. W. Edmonds *et al.*, Appl. Phys. Lett. **86**, 152114 (2005).
[8] N. Zainal, S. V. Novikov, C. J. Mellor, C. T. Foxon, and A. J. Kent, Appl. Phys. Lett. **97**, 112102 (2010).
[9] C. Mietze, K. Lischka, and D. J. As, Phys. Status Solidi A **209**, 439 (2012).
[10] D. J. As *et al.*, Appl. Phys. Lett. **76**, 1686 (2000).
[11] D. J. As and C. Mietze, Phys. Status Solidi A **210**, 474 (2013).
[12] L. X. Benedict and E. L. Shirley, Phys. Rev. B **59**, 5441 (1999).
[13] G. Onida, L. Reining, and A. Rubio, Rev. Mod. Phys. **74**, 601 (2002).
[14] F. Aryasetiawan and O. Gunnarsson, Reports on Progress in Physics **61**, 237 (1998).
[15] L. C. de Carvalho, A. Schleife, and F. Bechstedt, Phys. Rev. B **84**, 195105 (2011).
[16] F. Giustino, S. G. Louie, and M. L. Cohen, Phys. Rev. Lett. **105**, 265501 (2010).
[17] E. Cannuccia and A. Marini, Phys. Rev. Lett. **107**, 255501 (2011).
[18] E. Cannuccia and A. Marini, arXiv:1304.0072 [cond-mat.mtrl-sci] (2013).
[19] S. Poncé *et al.*, arXiv:1309.0729 [cond-mat.mtrl-sci] (2013).
[20] X. Gonze, P. Boulanger, and M. Côté, Annalen der Physik **523**, 168 (2011).
[21] P. Allen and V. Heine, J. Phys. C **9**, 2305 (1976).
[22] M. Cardona, Sci. Technol. Adv. Mater. **7**, S60 (2006).
[23] P. B. Allen and M. Cardona, Phys. Rev. B **27**, 4760 (1983).
[24] A. Marini, Phys. Rev. Lett. **101**, 106405 (2008).
[25] R. Mattuck, *A guide to Feynman diagrams in the Many-Body problem* (McGraw-Hill, New York, 1976).
[26] H. Fan, Phys. Rev. **78**, 808 (1950).
[27] S. Botti and M. A. L. Marques, Phys. Rev. Lett. **110**, 226404 (2013).
[28] P. Giannozzi and al., J. Phys. Condens. Matter **21**, 395502 (2009).
[29] A. Marini, C. Hogan, M. Grüning, and D. Varsano, Comput. Phys. Comm. **180**, 1392 (2009).
[30] R. Del Sole and R. Girlanda, Phys. Rev. B **54**, 14376 (1996).
[31] A. Marini and R. Del Sole, Phys. Rev. Lett. **91**, 176402 (2003).
[32] R. Armiento and A. E. Mattsson, Phys. Rev. B **72**, 085108 (2005).
[33] J. Heyd, G. E. Scuseria, and M. Ernzerhof, The Journal of Chemical Physics **118**, 8207 (2003).
[34] S. Logothetidis, J. Petalas, M. Cardona, and T. D. Moustakas, Phys. Rev. B **50**, 18017 (1994).